Anal. Chem. **2003,** *75,* 3643−3649

Portable High-Voltage Power Supply and Electrochemical Detection Circuits for Microchip Capillary Electrophoresis

Douglas J. Jackson,[†] John F. Naber,[†] Thomas J. Roussel, Jr.,[‡] Mark M. Crain,[†] Kevin M. Walsh,[†] Robert S. Keynton,[‡] and Richard P. Baldwin*[,§]

Department of Electrical and Computer Engineering, Department of Chemistry, and Department of Mechanical Engineering, University of Louisville, Louisville, Kentucky 40292

Miniaturized, battery-powered, high-voltage power supply, electrochemical (EC) detection, and interface circuits designed for microchip capillary electrophoresis (CE) are described. The dual source CE power supply provides ±1 kVDC at 380 μA and can operate continuously for 15 h without recharging. The amperometric EC detection circuit provides electrode potentials of ±2 VDC and gains of 1, 10, and 100 nA/V. The CE power supply power is connected to the microchip through an interface circuit consisting of two miniature relays, diodes, and resistors. The microchip has equal length buffer and separation channels. This geometry allows the microchip to be controlled from only two reservoirs using fixed dc sources while providing a consistent and stable sample injection volume. The interface circuit also maintains the detection reservoir at ground potential and allows channel currents to be measured likewise. Data are recorded, and the circuits are controlled by a National Instruments signal interface card and software installed in a notebook computer. The combined size (4 in. × 6 in. × 1 in.) and weight (0.35 kg) of the circuits make them ideal for lab-on-a-chip applications. The circuits were tested electrically, by performing separations of dopamine and catechol EC and by laser-induced fluorescence visualization.

Recent work in the area of chip-based capillary electrophoresis (CE) has focused nearly exclusively on issues related to fabrication of the microchip devices and characterization of their operation and analytical performance. As a result, many attractive features and important applications of microchip systems, mostly bioanalytical in nature, have been demonstrated.[1−4] These microchip CE experiments have nearly always been performed with conventional benchtop high-voltage (HV) power supplies, and the detection scheme most commonly employed has consisted of laser-induced fluorescence (LIF) systems usually designed for conventional capillary CE instruments. Thus, despite the high degree of miniaturization accomplished for the CE platform as a consequence of the microfabrication approach, the entire CE instrument has certainly not been miniaturized to the same extent. For some applications (such as high-speed DNA sequencing), this probably does not represent a severe limitation. However, it does serve to hinder many potential applications where instrument portability is essential—such as remote environmental monitoring, on-site sensing of chemical or biological agents, and point-of-care medical diagnostics.

Although LIF and other optical approaches do present significant opportunities for "whole system" miniaturization,[5−7] on-chip electrochemical (EC) detection methodologies, in which the detection electrodes are integrated directly onto the CE chip during microfabrication, would seem to offer an alternative that is more ideally suited to this end. In point of fact, several laboratories have demonstrated EC detection, usually amperometric in nature, to be viable and attractive for lab-on-a-chip systems.[8−25] In a previous paper,[25] our group has described the

* Corresponding author. E-mail: rick.baldwin@louisville.edu. Fax: (502) 852-8149.

[†] Department of Electrical and Computer Engineering.

[‡] Department of Mechanical Engineering.

[§] Department of Chemistry.

(1) Service, R. F. *Science* **1998**, *282*, 396−401.
(2) Figeys, D.; Pinto, D. *Anal. Chem.* **2000**, *72*, 330A−335A.
(3) Reyes, D. R.; Iossifidis, D.; Auroux, P.-A.; Manz, A. *Anal. Chem.* **2002**, *74*, 2623−2636.
(4) Auroux, P.-A.; Iossifidis, D.; Reyes, D. R.; Manz, A. *Anal. Chem.* **2002**, *74*, 2637−2652.
(5) Burns, M. A.; Johnson, B. N.; Brahmasandra, S. N.; Handique, K.; Webster, J. R.; Krishnan, M.; Sammarco, T. S.; Man, P. M.; Jones, D.; Heldsinger, D.; Mastrangelo, C. H.; Burke, D. T. *Science* **1998**, *282*, 484−487.
(6) Schwarz, M. A.; Hauser, P. C. *Lab Chip* **2001**, *1*, 1−6.
(7) Chabinyc, M. L.; Chiu, D. T.; McDonald, J. C.; Stroock, A. D.; Christian, J. F.; Karger, A. M.; Whitesides, G. M. *Anal. Chem.* **2001**, *73*, 4491−4498.
(8) Woolley, A. T.; Lao, K.; Glazer, A. N.; Mathies, R. A. *Anal. Chem.* **1998**, *70*, 684−688.
(9) Wang, J.; Tian, B.; Sahlin, E. *Anal. Chem.* **1999**, *71*, 3901−3904.
(10) Wang, J.; Tian, B.; Sahlin, E. *Anal. Chem.* **1999**, *71*, 5436−5440.
(11) Wang, J.; Chatrathi, M. P.; Tian, B. *Anal. Chem.* **2001**, *73*, 1296−1300.
(12) Wang, J.; Chatrathi, M. P.; Mulchandani, A.; Chen, W. *Anal. Chem.* **2001**, *73*, 1804−1808.
(13) Wang, J.; Pumera, M.; Chatrathi, M. P.; Escarpa, A.; Musameh, M.; Collins, G.; Mulchandani, A.; Lin, Y.; Olsen, K. *Anal. Chem.* **2002**, *74*, 1187−1191.
(14) Henry, C. S.; Zhong, M.; Lunte, S. M.; Kim, M.; Bau, H.; Santiago, J. J. *Anal. Commun.* **1999**, *36*, 305−307.
(15) Martin, R. S.; Gawron, A. J.; Lunte, S. M.; Henry, C. S. *Anal. Chem.* **2000**, *72*, 3196−3202.
(16) Gawron, A. J.; Martin, R. S.; Lunte, S. M. *Electrophoresis* **2001**, *22*, 242−248.
(17) Martin, R. S.; Ratzlaff, K. L.; Huynh, B. H.; Lunte, S. M. *Anal. Chem.* **2002**, *74*, 1136−1143.
(18) Rossier, J. S.; Roberts, M. A.; Ferrigno, R.; Girault, H. H. *Anal. Chem.* **1999**, *71*, 4294−4299.
(19) Rossier, J. S.; Schwarz, A.; Reymond, F.; Ferrigno, R.; Bianchi, F.; Giraul, *72*t, H. H. *Electrophoresis* **1999**, *20*, 727−731.

10.1021/ac0206622 CCC: $25.00
Published on Web 06/07/2003

construction and characterized the performance of a microfabricated CE/EC device in which all CE and EC electrodes were incorporated onto the microchip photolithographically. In the present study, we extend our earlier work by describing the design and operation of miniaturized CE and EC electronics intended to support this device and foster the development of a self-contained, transportable CE instrument.

There have been a few reports involving the development of such miniaturized or portable CE/EC instrumentation. Most notably, Hauser's group has described the construction of a battery-powered, field-portable CE instrument capable of carrying out amperometric, potentiometric, and conductivity detection.[26,27] However, this approach, which employed a conventional fused-silica capillary for separation, was not intended for microchip-level application. In addition, Martin et al.[17] reported a miniaturized battery-powered potentiostat circuit for amperometric detection in lab-on-a-chip CE/EC systems but used a conventional benchtop CE power supply. In our current work, our goal has been to develop a complete electronics package, including both CE and EC operations, that is targeted specifically for microchip analysis systems. In particular, we have developed both a portable battery-powered dual-source high-voltage power supply that allows independent voltage control of both the CE injection and separation channels on the microchip and a battery-powered potentiostat for potential control and current monitoring for amperometric EC detection.

EXPERIMENTAL SECTION

The discussion below is intended primarily to address the principles of design and operation of the new CE and EC circuits developed here. Detailed circuit schematics are available electronically on request.

APPARATUS

Microfabricated CE Devices. The layout of the CE/EC microchip device (shown in Figure 1), and the fabrication procedures employed have been described in detail previously.[25] Therefore, only a basic overview of these topics is provided here. Two intersecting 50 μm wide × 20 μm deep × 2 cm long channels for sample loading and separation were wet etched into a 2 in. × 2 in. soda lime glass substrate that formed the top half of the device. Reservoirs were then formed by drilling holes at the channel ends using a diamond core drill bit. Platinum CE and EC electrodes were photolithographically patterned onto a second glass section. The two substrates were then visually aligned and thermally bonded under compression at 650 °C. An acrylic fixture with

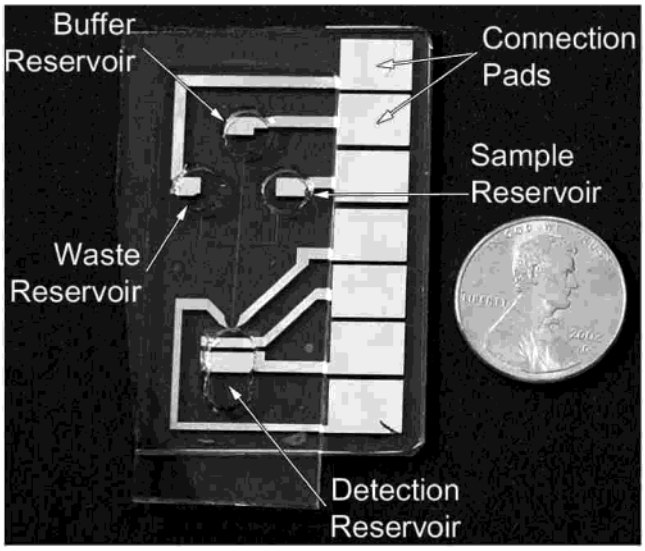

Figure 1. Balanced cross geometry CE chip with integrated Pt CE and detection electrodes.

spring-loaded contacts was used to hold the microchip in place and make electrical connection to the platinum connection pads for the CE and EC electrodes. An important aspect of the device was its "balanced cross" geometry in which the buffer and separation channels were equal in length. With this arrangement, the physical and electrical properties of the channels were balanced so that a well-defined sample plug was formed at the channel intersection without special adjustments of the CE potentials.[28]

CE/LIF experiments were performed on a second microfabricated chip possessing a CE channel structure identical to that above; however, the lower half consisted of an unpatterned glass substrate with no electrodes. Consequently, this particular device employed externally positioned Pt wires as CE electrodes.

High-Voltage Power Supply. The portable battery-powered dual-source HV power supply (Figure 2a) was designed using EMCO High Voltage Corp. (Sutter Creek, CA) Q series dc-to-dc converter modules as HV sources. These modules, which are available with output voltages ranging from ±250 VDC to ±10 kVDC at 0.5 W, are ideal for portable battery-powered operation because they are small (0.125 in.^{3}), lightweight (0.15 oz), and require only a 5-VDC input voltage. In addition, the nonswitching topology of the converter generates very low output ripple and electromagnetic interference. Nevertheless, in view of the nanoampere level of the currents encountered in amperometric EC detection, an RC filter and a copper foil shield were added to provide a further reduction in noise.

For this specific design, the Q12-5 and Q12-5N modules, which are rated at +1.2 and −1.2 kVDC at 400 μA, respectively, were chosen. Power was supplied by four AA-size rechargeable 1300 mAH NiMH batteries. Although the dc-to-dc converter output voltage is proportional to the input voltage, the modules themselves do not contain any internal voltage regulation. Therefore, to compensate for varying loads and battery discharge and to make the output voltage adjustable, a closed-loop regulation circuit was included for each source. The batteries and circuitry were placed onto a custom-made 3 in. × 4 in. double-sided FR4 printed circuit board.

(20) Rossier, J. S.; Ferrigno, R.; Girault, H. H. *J. Electroanal. Chem.* **2000**, *492*, 15−22.
(21) Hilmi, A.; Luong, J. H. T. *Anal. Chem.* **2000**, *72*, 4677−4682.
(22) Tantra, R.; Manz, A. *Anal. Chem.* **2000**, *72*, 2875−2878.
(23) Schwarz, M. A.; Galliker, B.; Fluri, K.; Kappes, T.; Hauser, P. C. *Analyst* **2001**, *126*, 147−151.
(24) Guijt, R. M.; Baltussen, E.; van der Steen, G.; Schasfoort, R. B. M.; Schlautmann, S.; Billiet, H. A. H.; Frank, J.; van Dedem G. W. K.; van den Berg, A. *Electrophoresis* **2001**, *22*, 235−241.
(25) Baldwin, R. P.; Roussel, T. R., Jr.; Crain, M. M.; Bathlagunda, V.; Jackson, D. J.; Gullapalli, J.; Conklin, J. A.; Pai, R.; Naber, J. F.; Walsh, K. M.; Keynton, R. S. *Anal. Chem.* **2002**, *74*, 3690−3697.
(26) Kappes, T.; Schnierle, P.; Hauser, P. C. *Anal. Chim. Acta* **1999**, *393*, 77−82.
(27) Kappes, T.; Galliker, B.; Schwarz, M. A.; Hauser, P. C. *Trends Anal. Chem.* **2001**, *20*, 133−139.
(28) Jacobson, J. C.; Ramsey, J. M. *Anal. Chem.* **1997**, *69*, 3212−3217.

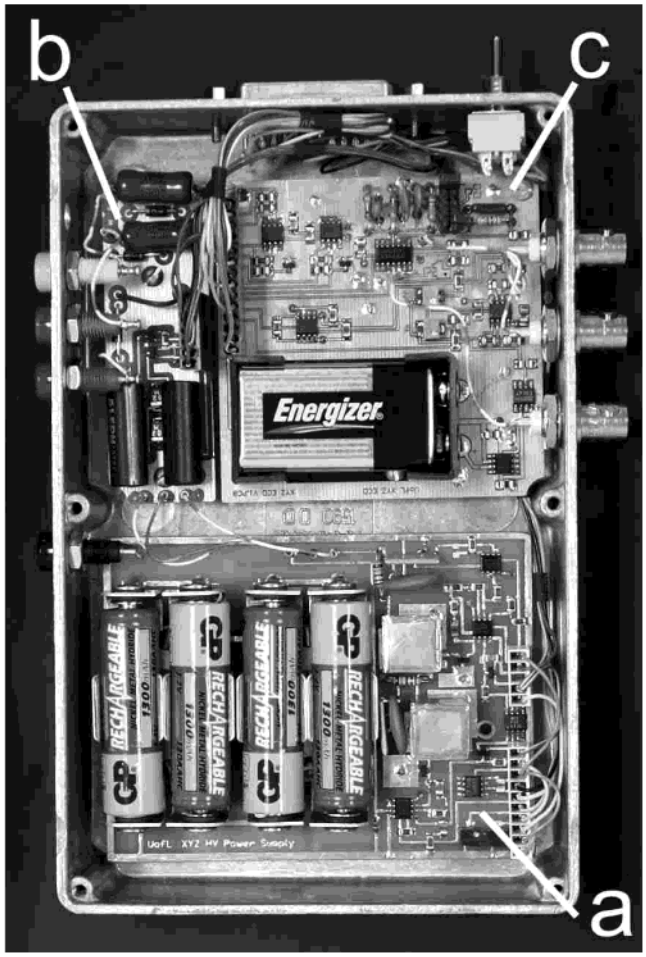

Figure 2. (a) Dual-source high-voltage power supply, (b) interface circuit, and (c) amperometric detection circuit.

The power supply was connected to the CE chip through the interface circuit (Figure 3) constructed on a 1 in. × 3 in. printed circuit board (Figure 2b). The ammeter circuits used to measure channel currents were included on the EC detection circuit board (Figure 2c). The power supply and interface circuit were both controlled with a National Instruments (Austin, TX) model DAQ 500 input−output (I/O) card and LabView software.

Channel Interface Circuit and Control. Because of the "balanced cross" geometry employed in fabricating the CE channels, CE operation required only that the waste and buffer reservoirs be connected to the HV power supply. As shown in Figure 3, this approach simplified the design of the interface circuit and minimized the number of HV sources required. More importantly, no adjustment of the CE potential was required to form and maintain a stable pinched sample plug at the channel intersection.

As with most CE chips, this design had two modes of operation: sample loading and injection/separation. In the sample loading mode, relay L1 was open and L2 closed (Figure 3), thereby connecting the negative HV source (V2) to the waste reservoir. In this mode, the buffer and sample reservoirs were connected to ground through forward-biased diodes D3 and D2 in series with ammeter circuits while the detection reservoir was directly connected to ground. As a result, buffer flowed from the three grounded reservoirs to the waste reservoir at equal rates due to the equal electric fields. The balanced buffer and separation channel flow produced the desired pinched sample flow at the channel intersection and prevented sample leakage into the detection or buffer channels.

In the injection/separation mode, the relays were toggled in order to connect the positive HV source (V1) to the buffer reservoir. In this mode, only the detection reservoir remained at ground potential while the sample and waste reservoirs were at the potential determined by the voltage drop across the 200 MΩ resistors R1 and R2. This voltage drop reduced the field in the waste and sample channels somewhat so that buffer flow was primarily directed from the buffer reservoir toward the detection reservoir. At the same time, a smaller flow was maintained to the waste and sample reservoirs in order to prevent leakage of sample

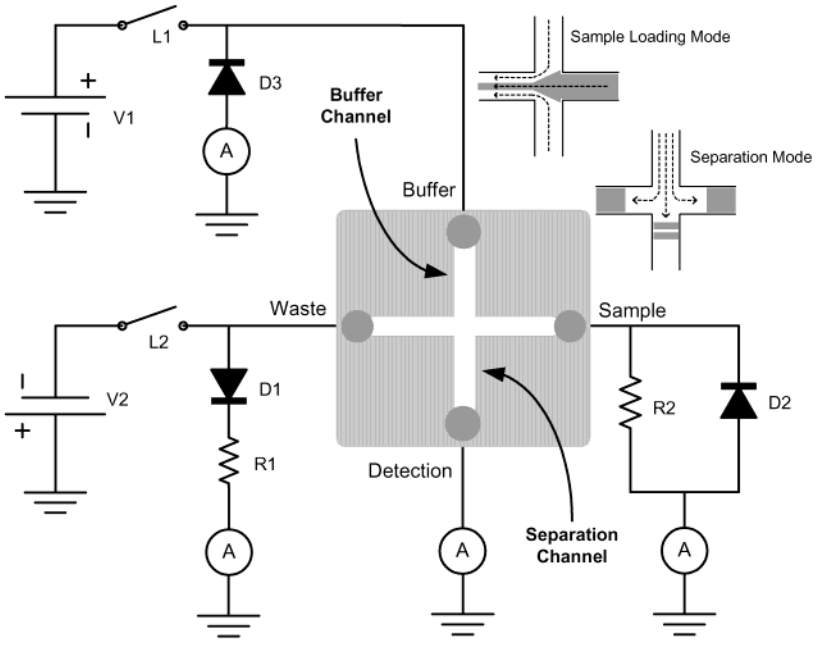

Figure 3. Interface circuit connecting high-voltage power supply to CE microchip.

into the separation channel during the CE separation. For both operational modes, the voltage at the channel intersection could be calculated from the currents measured in each channel segment using the assumption of equal resistance per unit length of the channels. This allowed the electric field strength of each channel to be determined.

Amperometric Electrochemical Detection Circuit. The EC detection electronics (Figure 2c) consisted of a potentiostat circuit and transimpedance (current-to-voltage) amplifier. Both circuits were designed using common operational amplifier integrated circuits (ICs) that were powered by a single 9-V battery whose output was split in order to provide a bipolar power source. Reference ICs provided stable voltage sources regardless of the battery charge. The working electrode was held at ground potential by a TLC2202 (Texas Instruments, Dallas, TX) operational amplifier connected as a single-stage transimpedance amplifier. Gain ranges of 1, 10, and 100 nA/V could be selected via the amplifier feedback resistance. A potentiometer connected to the amplifier input allowed for compensation of offset currents.

The working electrode potential could be varied over a range of ±2 VDC by using either an on-board potentiometer or an external signal to adjust the potentiostat. The potentiostat output was connected to one electrode that serves as both the auxiliary electrode and the CE cathode. The CE current was measured via an instrumentation amplifier that monitored the voltage drop across a 1 kΩ resistor in series with the auxiliary electrode/CE cathode. Thus, the measured current was actually the sum of the EC and CE currents. However, under nearly all operating conditions, the EC current was negligible as the CE current was larger by several orders of magnitude.

The EC detection circuitry and 9-V battery were placed on a 3 in. × 3 in. printed circuit board. Three additional transimpedance amplifiers used for channel current measurements were also included on the EC detection board. Data were recorded at 50 samples/s using a National Instruments I/O card and customized LabView© software. A moving window average of 50 samples was performed on the recorded data using MathCad (MathSoft, Cambridge, MA) to reduce noise.

EXPERIMENTAL PROCEDURES

Electrical Performance. Electrical tests were performed on the CE power supply in order to define its performance quantitatively as summarized in Table 1. Each voltage source was tested separately due to slight differences in the design of the positive and negative source circuits. Fixed resistors were used to load the power supply output and ensure that the measured performance data would be valid for a wide range of channel loads. All tests were performed at room temperature.

The load resistance and charge level of the batteries affect the maximum output voltage of the power supply. Therefore, to ensure that the maximum output measurements reported were valid during the full discharge cycle of the batteries, a laboratory power supply set at 4.8 VDC was substituted for the NiMH cells to simulate an end-of-charge condition. Maximum output voltage measurements were made by adjusting the on-board potentiometer for maximum output while monitoring the power supply output with loads between 2.5 and 100 MΩ. The maximum output current was simply the dc-to-dc converter's capacity less the small amount of current (V/100 MΩ) used by the internal regulation

Table 1. Summary of Circuit Specifications

Physical Dimensions	
size	3 in. × 4 in. × 1 in. CE power supply 3 in. × 3 in. × 1 in. EC detection circuit 3 in. × 1 in. × 1 in. interface circuit
weight	0.35 kg combined weight (with batteries)
Power Supply Circuit	
CE maximum output voltage	870 VDC at 2.5 MΩ, 1360 VDC at 50 MΩ
CE maximum output current	380 μADC
power supply ripple	10 mVp-p at 2.5 MΩ,1 kVDC
power supply accuracy	<3.6%
power supply continuous operating time	15 h at 10 MΩ, 30 h at 100 MΩ
power supply steady-state regulation	<0.1% from 2.5 MΩ to 100 MΩ
power supply stored energy	<60 mJ/source
Detection Circuit	
working electrode applied potential	±2 VDC
amperometric detection gain ranges	1, 10, 100 nA/V
detection current offset range	±250 nA
EC detector continuous operating time	40 h

circuitry. The power supply was operated from fully charged NiMH cells for the remaining electrical tests and CE experiments.

Signals used to monitor and regulate the power supply output sources were derived from the internal 100 MΩ (1000:1) voltage dividers and amplifiers. The accuracy of these signals determined the accuracy of any output voltage settings. The signals were tested for accuracy by a comparing them to output measurements made with a precision 1% (1000:1) voltage divider and a digital voltmeter. The measurements were made at output voltages ranging from 250 to 1250 VDC, and the highest error value was used as the specification listed in Table 1.

The power supply must maintain the desired output voltage as load resistance varies. This steady-state regulation ability was measured by monitoring the output voltage of the power supply as the loading resistance was varied from 2.5 to 100 MΩ. Again, the highest error was reported as the specification.

As mentioned above, the Q series dc-to-dc converters generate very low ripple noise due to their circuit topology. Additionally, the RC low-pass filter is very effective at reducing ripple due to the high operating frequency of the converter (>200 kHz). To measure these low-voltage levels, an oscilloscope was connected through a 0.01-μF 2-kV capacitor in series with the power supply output. The charged capacitor was required to block the high dc voltage from the oscilloscope input and prevent damage. Measurements were taken with the power supply loaded with a 2.5 MΩ resistor and adjusted to ±1 kVDC.

The maximum operating time for the power supply was dependent on battery capacity and power supply load resistance. With fully charged 1300 mAH NiMH cells and power supply load resistances of 10 and 100 MΩ, the operating time was measured by logging the output voltage with LabView software. During normal CE operation, only one HV source is active at a time so the power supply was tested with only one source active.

LIF Imaging. The sample loading and injection processes were visualized using LIF to provide visual validation of the CE chip control approach. The CE chip was filled by adding phosphate buffer (20 mM, pH 4) to the CE cathode reservoir to fill the channel network by capillary action. Buffer was then added to

the waste and buffer reservoirs, and dichlorofluorescein (60 μM in phosphate buffer) was added to the sample reservoir. Platinum wires placed in each reservoir served as the CE electrodes. Since the separation channel current monitor is part of the potentiostat circuit, the potentiostat was connected by attaching the potentiostat reference signal lead and CE cathode-auxiliary electrode lead to the Pt wire in the CE cathode reservoir. This connection ensured that the potentiostat would operate in its linear range and provide channel current data. The channel currents were checked for symmetry in the sample loading and injection/separation modes. In the sample loading mode, the buffer, waste, and separation channels should carry equal currents. In the injection/separation mode, the waste and sample capillaries should have equal currents.

The CE chip was placed in the sample loading mode with −250 VDC applied to the waste reservoir. A 514-nm argon ion laser (∼35 mW) was introduced at roughly a 45-deg angle to the chip surface. After allowing 1 min for the sample channel to fill completely, an image of the channel intersection was captured using a 320 × 240 pixel CCD camera, 10× lens, and 570-nm cut-on filter. The chip was then placed in the separation mode by applying +250 VDC to the buffer reservoir. An image was captured immediately after the mode change.

Electrochemical Detection. The EC detection circuit was tested by performing separations of 2.2 mM dopamine and 4.6 mM catechol in 20 mM pH 6 phosphate buffer using the fully integrated CE/EC chip. The channels were filled and verified using the same procedure as above for LIF experiments. The chip was placed in the sample-loading mode for 1 min with the negative source set at −250 VDC. The separation mode was then selected with the working electrode potential set to +850 mV relative to the reservoir potential. Separations were performed at CE fields of 25, 50, 100, and 200 V/cm.

RESULTS AND DISCUSSION

Circuit Specifications and Performance. The objective of this work was the development of HV power supply and EC detection circuitry specifically designed for microchip-based CE instruments and the unique applications for which these devices might be utilized. This is desirable because most lab-on-a-chip studies have thus far tended to focus on microfabrication issues and have usually employed conventional benchtop CE power supplies and EC potentiostats to carry out device control and data acquisition functions. Of course, one of our principal aims was the miniaturization of the physical size of the power supply and supporting circuits in order to better match the size of the microfabricated CE/EC platform. It was also critical to minimize the power consumption of these support circuits in order to allow operation under battery power and facilitate possible remote or field usage. Apart from these obvious priorities, it is important to realize that the electronic requirements for chip-based CE, especially for the CE power supply, can be distinctly different from those for ordinary discrete CE. For example, because of the shorter CE channel lengths common to microchip instrumentation, lower power supply voltages are usually required to generate the same CE field strengths used in conventional CE instruments. In addition, chip-based CE, with its need for separate channels for sample loading and separation, may require multiple HV sources as well as specific HV switching and channel control capabilities to provide simultaneous (or easily adjustable) flow control in each channel. In all these considerations, our goal has been to develop a circuitry package that meets the particular needs of microchip CE/EC in a simple and cost-effective manner.

Table 1 summarizes the physical dimensions and electrical specifications of the circuitry package developed here. Clearly, its overall size (4 in. × 6 in. × 1 in.) and weight (<0.35 kg) are fully suitable for the lab-on-a-chip environment. In addition, with the four 1.5-V and one 9-V batteries used to power the CE and EC circuits, continuous operation over periods of at least 15 h was routinely achieved. The maximum CE voltage obtained was on the order of 1 kV, depending on the resistive loading provided by the specific CE channel and buffer conditions in effect, and with the 2-cm channel length employed (i.e., the total channel length between high-voltage CE anode and cathode on the microchip), CE field strengths as high as 500 V/cm could be achieved. In practice, CE voltages on the order of 200 VDC (and CE fields of ∼100 V/cm) were found suitable to provide fast separation of the analytes examined here and were typically used in most of the work described below. However, for microchip designs or CE applications requiring higher voltages, other EMCO model Q voltage converters could be substituted for the Q12 modules employed in the current device. Of course, for such higher voltage applications, the voltage tolerance of the supporting electrical components (including relays, filter capacitors, and diodes) would also need to be taken into consideration. The maximum available CE current, 400 μA, was well above the 100-μA levels typically encountered in microchip CE. Again, while it is doubtful that there would be a frequent need for higher currents than this, other converter modules with a greater current capacity output could be substituted.

The EC detection circuit provided sufficient working electrode potential (±2 VDC) and offset correction (±250 nA) for the experiments herein. Likewise, the gain ranges of the single-stage current to voltage converter (1, 10, 100 nA/V) were adequate for millimolar to micromolar detection levels. The moving window averaging improved the signal quality particularly on the 1 nA/V setting. If desired, this postprocessing step could be eliminated by adding an analog low-pass filter to the detector or by performing the averaging in real time.

Sample Loading and Injection. The initial microchip devices used in this work were fabricated with sample loading and separation channels that were equal in length but arranged nonsymmetrically so that their intersection point was closer to the buffer reservoir than to the detection reservoir. This approach, which maximizes both the channel length available for the CE separation and the fraction of the HV output available to drive it, is common practice in microchip CE/EC. However, while this arrangement is advantageous for the actual separation step, it complicates sample loading and injection by requiring individual adjustment of the potentials applied to the sample, waste, buffer, and detection reservoirs in order to create balanced flow of the streams at the channel intersection and the formation of a well-defined injection plug.

Of course, these problems could in principle be addressed in a variety of ways (e.g., by having separate HV sources for sample, buffer, and waste reservoirs and using either trial and error or LIF visualization to optimize flow patterns). However, the simplest

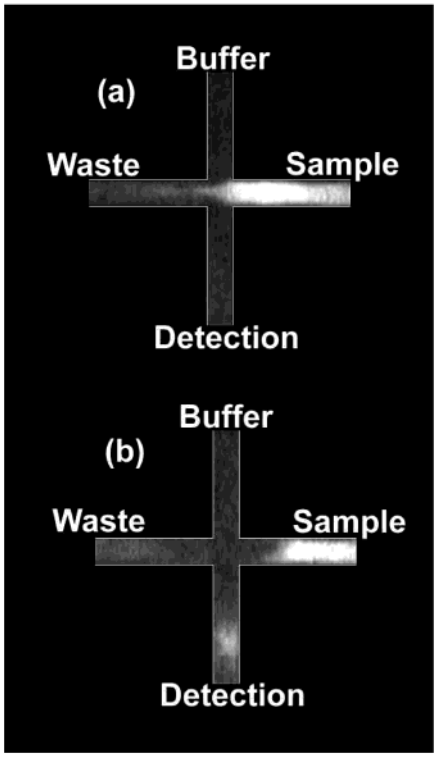

Figure 4. LIF images of dichlorofluorescein during (a) sample loading mode and (b) separation mode.

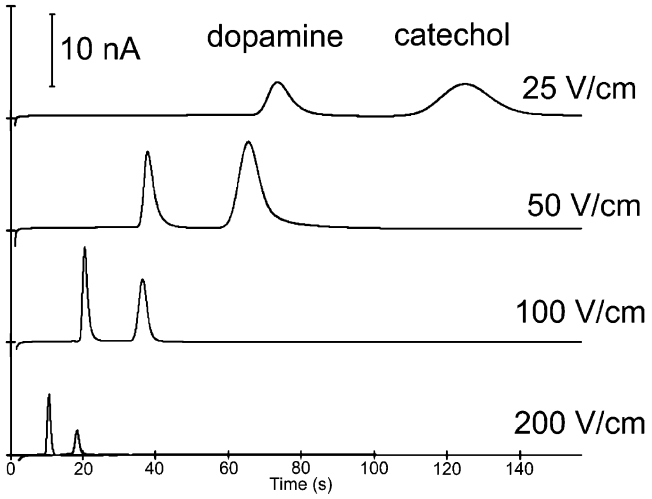

Figure 5. Separations of 2.2 mM dopamine and 4.6 mM catechol in 20 mM pH 6 phosphate buffer using Pt electrodes.

experimental solution by far involved switching to a symmetrical or balanced arrangement in which two channels intersect to form equal-length buffer and separation segments (see Figure 3). The microchip devices used in these experiments in fact consisted of four segments or "arms" that were dimensionally identical and electrically equivalent. It is, however, the equal-length buffer and separation channels that are key to the inherently balanced behavior. Consequently, all sample-loading and injection/separation operations (procedures described in detail in the Experimental Section) required only two independent HV sources, and there was no need for separate adjustment of the voltage applied to each reservoir. Most important, with this balanced channel geometry, it was possible to carry out the injection of a small well-defined sample plug.

Figure 4 shows LIF images obtained using this approach for the loading and injection of a dichlorofluorescein sample. Here it can be seen that, during the sample-loading phase (Figure 4a), the flow of the sample was clearly directed solely toward the waste with no apparent leakage in the direction of the buffer and separation channels. Close inspection of the channel intersection reveals the expected pinched flow pattern formed because, in this mode, equal flow from the buffer, sample, and separation channels is being directed toward the waste reservoir. This pattern was assumed shortly after starting sample loading by applying the appropriate HV to the waste reservoir and was maintained stably until this HV was removed. Sample injection was triggered by application of HV to the buffer reservoir and resulted in the flow pattern shown in Figure 4b. Here the increased flow from the buffer channel can clearly be seen to be clearing the sample and waste channels and pushing a small dichlorofluorescein plug toward the detection reservoir. This plug appears to have approximately the same volume as the channel intersection, and there is no apparent dichlorofluorescein leakage out of the sample and waste channels.

Practical advantages of the balanced channel design, important for simple circuit design and operation, include the fact that the CE detection reservoir remains at ground potential during the entire measurement process and the EC electrodes are never exposed to HV environments that would necessitate electrical isolation. Likewise, measurements of channel currents can be made relatively simply at ground potential conditions. Finally, for possible-high throughput applications, a parallel connection of multiple CE microchips and interface circuits could be driven by a single power supply system because the HV required for each would be exactly the same. As mentioned above, the principal disadvantage of the balanced channel approach is that slightly less than half of the CE power supply voltage is dropped across the separation capillary. While this has not proven to present any problem in the current work, there are straightforward alterations to the microchip design that could be adopted to make more efficient use of the HV source without compromising the quality of sample loading and injection. For example, during chip fabrication, a fifth reservoir or electrode could be placed along the buffer capillary near the intersection. This configuration would allow the CE voltage to be applied near the intersection while in the detection mode, but would allow the full length of the buffer capillary to be used to equalize flow while in the sample-loading mode.

CE/EC Performance. In a previous publication,[25] we described in detail the operation and performance of the microchip device used in this work. In particular, the microfabricated CE chip and integrated EC electrode system was shown to provide detection of test analytes dopamine and catechol down to low-micromolar levels and to give extraordinarily stable performance over months of routine use. In view of the fact that the electronics package described here is the same as that employed in the earlier study, it seems that there is no need to reproduce the same electropherograms and associated data here. Furthermore, in any practical application, the analytical performance obtained will be predominantly determined by the specific characteristics of the microchip platform (e.g., channel and electrode dimensions,

Table 2. CE Characteristics for Dopamine and Catechol as a Function of Applied CE Voltage[a]

applied CE field (V/cm)	migration time (s)	apparent mobility (μm·V/s)	peak area (arbitrary units)	efficiency (plates/m)
		Dopamine		
25	73.0 ± 0.5	55 200 (±490)	1510 (±73)	69 100 (±2300)
50	37.6 ± 0.1	53 700 (±180)	1520 (±66)	93 500 (±1900)
100	20.1 ± 0.1	51 000 (±530)	980 (±110)	98 900 (±1300)
200	10.5 ± 0.0	47 900 (±100)	435 (±15)	54 200 (±2000)
		Catechol		
25	124.6 (±1.0)	32 400 (±300)	3470 (±122)	28 000 (±800)
50	65.4 (±0.4)	30 900 (±230)	4050 (±136)	38 900 (±100)
100	36.0 (±0.1)	28 600 (±260)	1170 (±85)	68 000 (±800)
200	18.2 (±0.0)	27 800 (±130)	197 (±5)	100 400 (±5200)

[a] Values represent the average of three separate experiments; numbers shown in parentheses represent absolute standard deviations.

electrode placement, electrode material, etc.) rather than by the supporting circuitry.

Accordingly, we include here only one illustration of typical electropherograms obtained with our instrumental approach. This is provided in Figure 5, which shows the CE separation and EC detection of a dopamine/catechol mixture carried out at a Pt working electrode over CE field strengths ranging from 25 to 200 V/cm (or voltage outputs of roughly 50−400 VDC from the high-voltage CE circuit). Relevant CE properties derived from these electropherograms are summarized in Table 2. In all cases, the EC signal quickly returned to baseline within a few seconds after sample injection was initiated by switching the HV to the buffer reservoir, although the time required for this did increase slightly for the higher CE voltages. Migration times for both compounds decreased, as expected, as the CE voltage was increased. Under the specific conditions in effect for this set of experiments, the detection limit was in the 4 μM range for all CE voltages examined. So it seems clear that the CE and EC circuitry was able to carry out basic injection, separation, and detection operations effectively. Peak sizes (both heights and areas) obtained for both dopamine and catechol were generally seen to decrease at higher CE voltages. While there were undoubtedly several different experimental factors that contributed to this phenomenon (e.g., higher flow rates prevailing at higher CE fields), it seems likely that smaller sample volumes were injected at the higher separation voltages. Interestingly, this effect did not occur equally for the two analytes. Rather, variations in peak size seemed to be much greater for the uncharged catechol than for the positively charged dopamine. While this phenomenon will continue to be the subject of study in our laboratory, it is apparent that specific HVs used during sample loading and separation steps can have significant consequences on injection volumes.

CONCLUSION

Microfabrication has made the portable CE/EC device practical. As field applications for these devices emerge, portable analysis systems will need to be developed. The results presented in this paper demostrate that miniaturization of the required electronics is also practical.

During the development of the system, it became apparent that the design of the electronics is highly dependent on the design of the microfabricated device. The vast design flexibility permitted by microfabrication makes a universal power supply and detector design challenging. While it would be possible for power supply and detection circuits to be designed to encompass a wide range of CE/EC device designs, the approach would not produce optimal results in size, cost, and performance. Additionally, most field applications will be unique and justify a specific CE/EC microchip design and electronics.

ACKNOWLEDGMENT

This work was supported by the National Science Foundation XYZ-on-a-Chip program under Grant CTS-9980831 and by the Department of Energy under Grant 46411101095.

Received for review October 24, 2002. Accepted April 8, 2203.

AC0206622